Foam-Oil Displacements in Porous Media
Insights from Three-Phase Fractional-Flow Theory

Tang, Jinyu; Castaneda, Pablo; Marchesin, Dan; Rossen, William R.

DOI
10.2118/211467-MS

Publication date
2022

Document Version
Final published version

Published in
Society of Petroleum Engineers - ADIPEC 2022

SPE-211467-MS

Foam-Oil Displacements in Porous Media: Insights from Three-Phase Fractional-Flow Theory

Jinyu Tang, United Arab Emirates University; Pablo Castaneda, Mexico Autonomous Institute of Technology, ITAM; Dan Marchesin, National Institute of Pure and Applied Mathematics, IMPA; William R. Rossen, Delft University of Technology

 DOI 10.2118/211467-MS

This paper was prepared for presentation at the ADIPEC held in Abu Dhabi, UAE, 31 October – 3 November 2022.

Abstract

Foam is remarkably effective in the mobility control of gas injection for enhanced oil recovery (EOR) processes and CO_2 sequestration. Our goal is to better understand immiscible three-phase foam displacement with oil in porous media. In particular, we investigate (i) the displacement as a function of initial (I) and injection (J) conditions and (ii) the effect of improved foam tolerance to oil on the displacement and propagation of foam and oil banks.

We apply three-phase fractional-flow theory combined with the wave-curve method (WCM) to find the analytical solutions for foam-oil displacements. An n-dimensional Riemann problem solver is used to solve analytically for the composition path for any combination of J and I on the ternary phase diagram and for velocities of the saturations along the path. We then translate the saturations and associated velocities along a displacement path to saturation distributions as a function of time and space.

Physical insights are derived from the analytical solutions on two key aspects: the dependence of the displacement on combinations of J and I and the effects of improved oil-tolerance of the surfactant formulation on composition paths, foam-bank propagation and oil displacement. The foam-oil displacement paths are determined for four scenarios, with representative combinations of J and I that each sustains or kills foam. Only an injection condition J that provides stable foam in the presence of oil yields a desirable displacement path, featuring low-mobility fluids upstream displacing high-mobility fluids downstream. Enhancing foam tolerance to oil, e.g. by improving surfactant formulations, accelerates foam-bank propagation and oil production, and also increases oil recovery. Also, we find a contradiction between analytical and numerical solutions. In analytical solutions, oil saturation (S_o) in the oil bank is never greater than the upper-limiting oil saturation for stable foam (*fmoil* in our model). Nevertheless, in numerical simulations, S_o may exceed the oil saturation that kills foam in the oil bank ahead of the foam region, reflecting a numerical artifact. This contradiction between the two may arise from the calculation of pressure and pressure gradient using neighboring grid blocks in a numerical simulation.

The analytical solutions we present can be a valuable reference for laboratory investigation and field design of foam for gas mobility control in the presence of oil. More significantly, the analytical solutions,

which are free of numerical artifacts, can be used as a benchmark to calibrate numerical simulators for simulating foam EOR and CO2 storage processes.

Introduction

Gas injection into geological formations, e.g. aquifers or oil reservoirs, is subject to very poor sweep efficiency (Glass and Yarrington, 2003; Reynolds and Krevor, 2015). Foam can increase remarkably the sweep efficiency of gas injection by reducing gas mobility, e.g. by an order of 10 ~ 10^6 (Schramm, 1994; Rossen, 1996). This allows broad engineering applications of foam in various subsurface processes: enhanced oil recovery (Rossen, 1996; Lake et al., 2014); acid diversion in well stimulation (Zhou and Rossen, 1995); removal of NAPL (Non-Aqueous Phase Liquid) contaminants in soils and aquifers (Estrada et al., 2015; Bertin et al., 2017); and carbon storage in CCUS (Carbon Capture, Utilization and Storage) (Bui et al., 2018; Castaneda-Herrera et al., 2018; Rossen et al., 2022).

Investigation of foam flow with oil or other NAPL's is perplexing both experimentally and numerically, due to the complex foam-oil interactions (Farajzadeh et al., 2012). Experimental studies demonstrate that foam flow without oil in porous media shows two regimes depending on foam quality, f_g, i.e. gas volumetric fractional flow in foam (Osterloh and Jante, 1992; Alvarez et al., 2001): the high- and low-quality regimes. Tang et al. (2019a) find that these two regimes also apply for foam with oil, as illustrated in the steady-state data of Fig. 1a (with no oil) and Fig. 2a (with oil). The presence of oil affects both regimes; this is implied by the shift of pressure-gradient $\#_p$ contours in each regime between Fig. 1a without oil and Fig. 2a with oil. Tang et al. also conducted a data fitting as shown in Figs. 1b and 2b using the STARS model (Computer Modeling Group, 2015). The agreement between data and fitted results not only justifies the suitability of the STARS model for representing foam flow with and without oil, but also reveals the foam-oil interaction mechanisms. In the upper-left high-quality regime, oil destabilizes foam through its effect on the limiting capillary pressure that corresponds to the limiting water saturation around which foam collapses (Zhou and Rossen, 1995). In the lower-right low-quality regime, oil weakens foam through its effect on a reference gas-mobility-reduction factor *fmmob*. (The STARS model does not fit the upward-tilting $\#_p$ contours in the low-quality regime in Fig. 1a (see also Kim et al., 2005). No currently applied foam simulation model yet accounts for this aspect of foam behavior.)

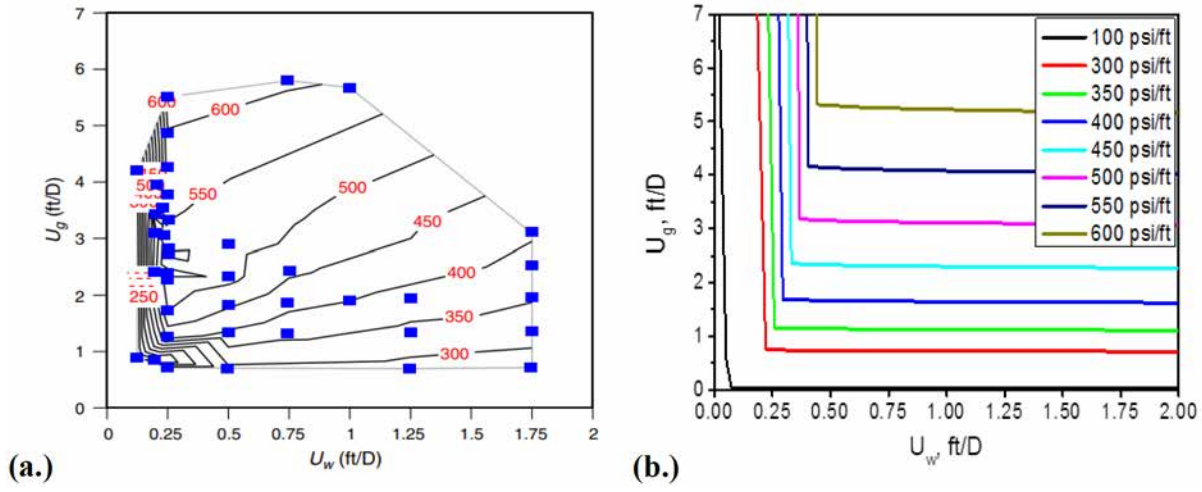

Figure 1—Pressure gradient (psi/ft) without oil as a function of gas (u_g) and water (uw) superficial velocities in a Bentheimer core of 1.98 Darcy: (a) steady-state data; (b) STARS model fit to data in Fig. 1a. Results from Tang et al. (2019a).

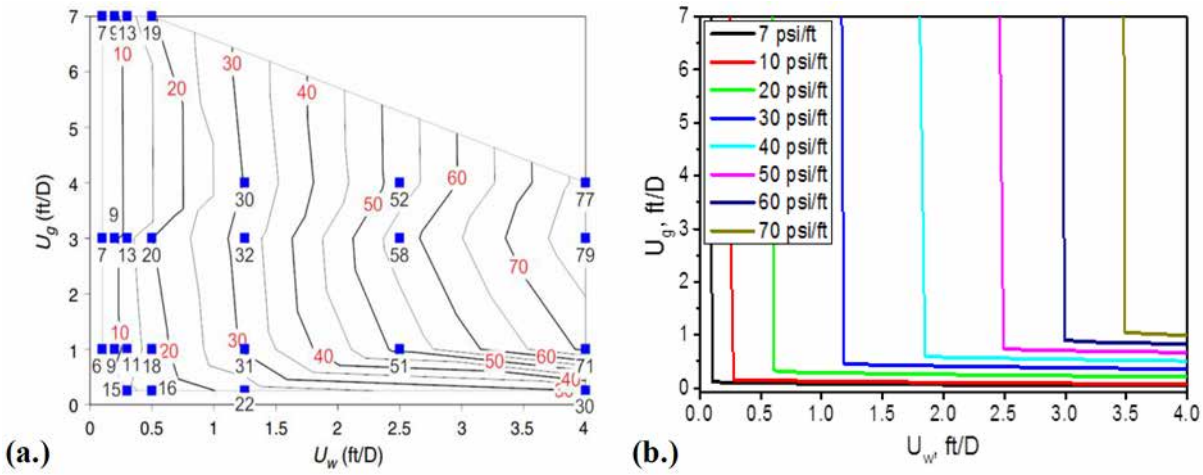

Figure 2—Pressure gradient (psi/ft) with oil as a function of gas (u_g) and water (uw) superficial velocities in a Bentheimer core of 1.98 Darcy: (a) steady-state data; (b) STARS model fit to data in Fig. 2a. Oil is introduced by fixing oil/water superficial velocity ratio at 0.25. Results from Tang et al. (2019a).

The two foam-flow regimes provide a simple and effective way to represent foam in porous media and its interactions with other factors. Foam-simulation-model parameters are estimated by data fitting to the two regimes. However, simulating complex multiphase-flow system such as foam faces a number of numerical challenges in (Rossen, 2013).

Fractional-flow theory, also called the Method of Characteristics (MOC), is a powerful analytical tool, revealing multi-phase flow behavior in porous media (Charbeneau, 1988; LaForce and Johns, 2005; Rossen et al., 2011; You et al., 2015). We apply this theory together with the wave-curve method (WCM) (Castaneda et al., 2016) to three-phase flow with foam represented with STARS model given in Appendix A. Our goal is to reveal the characteristics of foam flow with oil upon injection (J) and initial (I) conditions and investigate the effects of foam tolerance to oil on propagation velocities of foam and of oil banks.

The analytical solutions we present would guide the interpretation of phase mobilities, interactions and distributions in foam injection. In addition, the analytical solutions, which are free of numerical artifacts, can be used as important benchmarks for calibrating numerical simulators for foam-flow processes, e.g. Lyu et al. (2021).

Fractional-flow Theory and Foam Model

Three-phase fractional-flow theory

The system of foam flow with oil involves three phases (i.e. water, oil and gas) and interactions between foam and oleic phases. Solving analytically for a three-phase flow with all factors considered is mathematically a challenge. For the purpose of this study, the system is simplified as follows:

- flow is one dimensional;
- fluids and rock are both incompressible;
- gravity effects can be ignored;
- all phases are immiscible;
- the process is isothermal;
- no dispersive processes are considered (e.g. diffusion, dispersion, and capillary-driven flow);
- local equilibrium is attained immediately;

- all phases have Newtonian rheology;
- surfactant concentration is uniform in the aqueous phase everywhere.

Crucially, in this initial study there is no phase-behavior advantage for oil mobilization, e.g. no oilswelling by gas, stripping of oil into gas, or gas-oil miscibility. For such a process, mobility control is the key to improving sweep efficiency and delivering gas to zones where these advantages can work. Ashoori et al. (2010) examined the case of foam with first-contact miscible oil displacement, where only two phases are present at any location.

With the above assumptions, the system is governed by two independent mass-conservation equations:

$$\varphi\frac{\partial S_w}{\partial t}+u\frac{\partial f_w}{\partial x}=0 \tag{1}$$

$$\varphi\frac{\partial S_o}{\partial t}+u\frac{\partial f_o}{\partial x}=0 \tag{2}$$

where φ is the rock porosity, S_w and S_o are the water and oil saturations, x and t, are the position and time, and u is the total superficial velocity of the three phases. Fractional flow of phases is defined as

$$f_j=\frac{u_j}{u}, \tag{3}$$

where subscript j = w, o or g denoting water, oil or gas, and u_j is the Darcy velocity of phase j. f_j, representing the fractional flow of a phase, is one key concept in fractional-flow theory.

Darcy velocity uj is governed by Darcy's law:

$$u_i=\frac{kk_{rj}}{\mu_j}|\nabla p|, \tag{4}$$

where k is the absolute permeability of a medium, kj is the relative permeability of phase j, ft is the viscosity of phase j, $|\nabla p|$ is the magnitude of pressure gradient. The relative permeability kj of phase j is assumed here to be a function of only its own phase saturation, given by a Corey-type model:

$$k_{rj}=k_{rj}^0\left(\frac{S_{j,a}-S_{jr}}{1-S_{wc}-S_{or}-S_{gr}}\right)^{n_j} \tag{5}$$

Where k_{rj}^0 is the endpoint relative permeability to phase j, $S_{j,a}$ is the absolute saturation of phase j and S_{jir} is the residual saturation of phase j (e.g. S_{wc}, S_{or} or Sgr), and n_j is the Corey exponent.

Given that $u = u_w + u_o + u_g$, substituting Eq. 4 into Eq. 3 for phase j, transforms fj to:

$$f_i=\frac{k_{rj}/\mu_j}{k_{rw}/\mu_w+k_{ro}/\mu_o+k_{rg}^f/\mu_g}, \tag{6}$$

where (k_{rj}/μ_j) represents the relative mobility of phase j, and k_{rg}^f is the effective gas relative permeability, with superscript f denoting the presence of foam. In our modeling, only the k_{rg} function is affected by foam (See Eq. A-1 in Appendix A), with k_{rw} and k_{ro} functions unaffected. This assumption is justified experimentally and facilitates foam-flow modeling (Rossen, 1996; Schramm, 1994). The foam model is then coupled with fractional-flow model via k_{rg}^f in Eq. A-1, where krg is modified by a mobility-reduction factor FM in Eq. A-2. FM includes F_2 in Eq. A-3 (a function of S_w) and F_3 in Eq. A-8 (a function of So). Therefore, f_j is a function of only saturations (S_w, S_o).

To simplify Eqs. 1 and 2, we introduce dimensionless position and time variables x_D and t_D:

$$x_D\equiv\frac{x}{L}, \tag{7}$$

$$t_D \equiv \frac{u \cdot t}{(1 - S_{wc} - S_{or} - S_{gr})L\varphi}, \tag{8}$$

where L is the reservoir length, and t_D is the number of movable pore volumes injected. S_j is the saturation of phase j, normalized by the total movable saturation:

$$S_j \equiv \frac{S_{j,a} - S_{jr}}{(1 - S_{wc} - S_{or} - S_{gr})}. \tag{9}$$

Using Eqs. 7, 8 and 9, the system of Eqs. 1 and 2 is simplified to

$$\frac{dS}{dt_D} + \frac{dF}{dx_D} = 0 \tag{10}$$

where capitals S and F are vectors of $\begin{pmatrix} S_w \\ S_o \end{pmatrix}$ and $\begin{pmatrix} f_w \\ f_o \end{pmatrix}$, respectively

Fractional-flow theory states that any pair of saturations S propagates through a permeable medium with a given velocity as a function of S. Solving for $S(x_D, t_D)$ then becomes a mathematical issue of solving for velocities of S along a displacement path on the phase diagram. The velocity of S is given by the derivative of water-, oil- or gas-phase fractional flow at that saturation (fractional-flow theory assumes equal velocity for S_w, S_o and S_g at each pair of S) (Lake et al., 2014):

$$\eta(S) \equiv \frac{dx_D}{dt_D} = \frac{\partial f_j}{\partial S_j}. \tag{11}$$

We use an n-dimensional Riemann problem solver (RPn) that implements the WCM to solve for a composition path connecting J to I and velocities of S along the path on the phase diagram (Liu, 1974; Azevedo et al., 2010; Castaneda et al., 2016; Tang et al., 2019c). In general, the WCM constructs a complete path by solving for two families of wave curves: a forward slow wave curve starting from J, and a backward fast wave curve initiating from I. The two families of wave curves usually cross, resulting in an intermediate state IJ at the intersection. A complete path follows the path from J to intermediate state IJ, and then to I. Shock waves along a path are solved through the Rankine-Hugoniot locus, based on a mass balance across the shock:

$$F(S) - F(S_I) = \sigma(S - S_I) \tag{12}$$

where S_I denotes the saturations at the initial state I, and a is the shock velocity from $5i$ to 5.

Based on the saturations along the path and their velocities, one can construct saturation distributions as a function of position and time, $S(x_D, t_D)$.

Foam Model

The STARS model includes two algorithms representing the effect of oil on foam, the "wet-foam" algorithm for the effect of oil on the low-quality regime and the "dry-out" algorithm for the effect of oil on the high-quality regime (Tang et al., 2019b). The wet-foam model (in Appendix A) is implemented in this initial study, but we believe results using the dry-out model would be similar.

In the STARS model, foam is represented via a mobility-reduction factor, FM in Eq. A-2, which reduces k_{rg} as in Eq. A-1. FM involves a series of functions $F_{1\text{-}6}$, accounting for the effects of influential factors on foam. We consider two key functions, F_2 in Eq. A-3 for the effect of Sw and $F3$ in Eq. A-8 for the effect of S_o. The arctangent function for F_2 is approximated here by a polynomial function in Eq. A-7, to facilitate the calculation of (d_F/d_S) in Eq. 11.

Figure 3 displays a foam-property map that is characterized by $(1/FM)$ in Eq. A-2 as a function of (S_w, S_o) in ternary saturation space. The values of $(1/FM)$ split the ternary diagram into two regions: the foam region with $(1/FM) > 1$, i.e. the colored lower-left patch, and the no-foam region with $(1/FM) =$ or ~ 1,

i.e. the white portion. The foam region is bounded by water- and oil-related parameters, e.g. limiting water saturation, *fmdry* in Eq. A-2 and lower- and upper-limiting oil saturation, *floil* and *fmoil* in Eq. A-8.

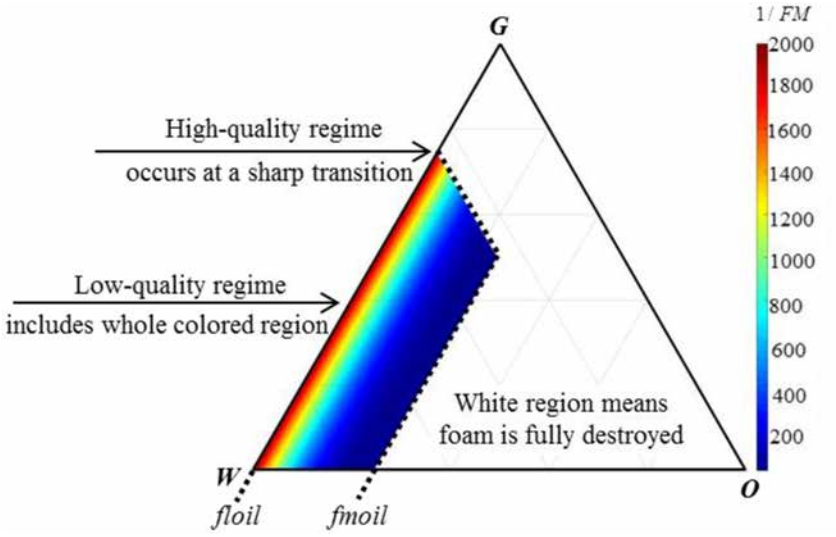

Figure 3—Gas-mobility-reduction factor (1/FM) in Eq. A-2 plotted as a function of (Sw, S_o) in ternary saturation space. The values of FM reflect F2 in Eq. A-7 and F3 in Eq. A-8, with parameters used given in Table A-1. The three vertices G, O, and W represent 100% normalized saturation (Eq. 9) of gas, oil and water, respectively. Thus, this and subsequent plots do not display residual phase saturations.

Along the direction parallel to gas-oil binary, for $S_w < (fmdry - \varepsilon)$ where $\varepsilon = 1/(2 \times epdry)$, foam is too dry to be maintained. For $(fmdry - \varepsilon) < S_w < (fmdry + \varepsilon)$, $(1/FM)$ rises suddenly and abruptly, corresponding to the high-quality regime in Figs. 1 and 2. For $S_w > (fmdry + \varepsilon)$, strong foam is present, corresponding to the low-quality regime. The transition between the two regimes corresponds to a transition zone in Fig. 3 within $(fmdry - \varepsilon) < S_w < (fmdry + \varepsilon)$, which is not visible here due to ε very small leading to a very sharp transition.

Parallel to gas-water binary, for $S_o < floil$, F_3 in Eq. A-8 equals unity, meaning that oil has no destabilizing effect on foam. For $floil < S_o < fmoil$, F_3 decreases with S_o, so does $(1/FM)$, due to a nonlinear destabilizing effect of oil on foam. For $S_o > fmoil$, $F_3 = 0$ and $(1/FM) = 1$, marking a foam destroyed completely by oil.

Results and Discussion

Table 1 summarizes the injection (J) and initial (I) conditions analyzed under four scenarios, with J and I each inside (denoted by subscript *fm*) or outside (denoted by subscript *nf*) the foam region as illustrated in Fig. 3. J_{nf} cannot maintain foam because it is too dry, whereas *Inf* kills foam completely because $S_o > fmoil$. For each case in Table 1, we solved for composition path, saturation velocities and distribution using three-phase fractional-flow theory combined with the WCM.

Table 1—A summary of *J* and *I* conditions used in fractional-flow analysis of foam flow with oil

Scenarios		Injection conditions 7= (5//)./	Initial conditions 7 =(&„&)	Foam model parameters
Scenario 1 (J_{nf} to I_{nf})	Case 1	J = (0.2, 0.8), f_g= 0.999	J = (0.1875, 0.8125)	Refer to Table A-l
Scenario 2 (J_{nf} to I_{fm})	Case 1	J = (0.2, 0.8). f_g =0.999	J = (0.7750, 0.2250)	Refer to Table A-l
Scenario 3 (J_{fm} to I_{fm})	Case 1	J= (0.3125, 0.6875), f_g = 0.195	J = (0.7750, 0.2250)	$fmoil$ = 0.25, $floil$ = 0, others from Table A-l
	Case 2	J = (0.3125, 0.6875), f_g = 0.195	J = (0.7750, 0.2250)	$fmoil$ = 0.5, $floil$ = 0, others from Table A-l

Scenarios		Injection conditions 7= (5//)./	Initial conditions 7 =(&,,&)	Foam model parameters
	Case 3	J= (0.3125, 0.6875), f_g = *0.195*	J = (0.7750, 0.2250)	*fmoil* = 0.5. *floil* = 0.2, others from Table A-1
Scenario 4 (J_{fm} to I_{nf})	Case 1	J = (0.3125, 0.6875), f_g = 0.195	J = (0.1875, 0.8125)	*fmoil* = 0.25, *floil* = 0, others from Table A-l
	Case 2	J= (0.3125, 0.6875), f_g = *0.195*	J = (0.1875, 0.8125)	*fmoil* = 0.5. *floil* = 0, others from Table A-l
	Case 3	J = (0.3125, 0.6875), f_g = *0.195*	J = (0.1875, 0.8125)	*fmoil* = 0.5, *floil* = 0.2, others from Table A-1

Note that (S_w, S_o) and *fmoil* and *floil* shown here are normalized using Eq. 9 for residual saturations.

Composition Paths of Foam Injection with Oil

Scenario 1 with Combination of J_{nf} and I_{nf}. Figure 4 shows the composition path for Case 1 of Scenario 1 for a combination of J_{nf} and I_{nf} both outside the foam region. S_w at J_{nf} is too low (too dry) to maintain foam, and S_o at I_{nf} is too high for foam to be stable. Nevertheless, the whole path bypasses the foam region, suggesting there is no foam occurring at all. Thus, this scenario also represents the composition path for co-injection of gas and water without surfactant.

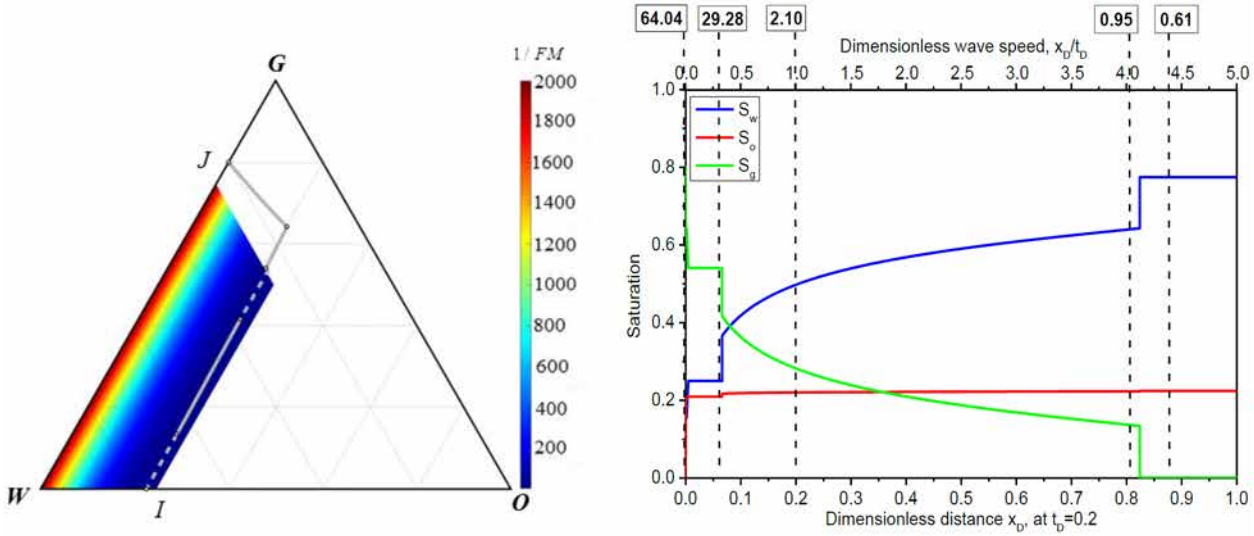

Figure 4—(Left). Composition path for Case 1 of Scenario 1 in Table 1 in ternary saturation space, with J_{nf} and *Inf* both outside the foam region. A solid line marks a spreading wave and a dashed line a shock.

The path starting from J_{nf} includes a spreading wave followed by a shock, and then a second spreading wave connected by a second shock to I_{nf}. Fundamentally, the path and wave type is a result of satisfying the velocity criterion of monotonically increasing from J to I (Lake et al., 2014). Only saturations along a spreading wave are physical which can appear in a displacement, as shown in Fig. 5.

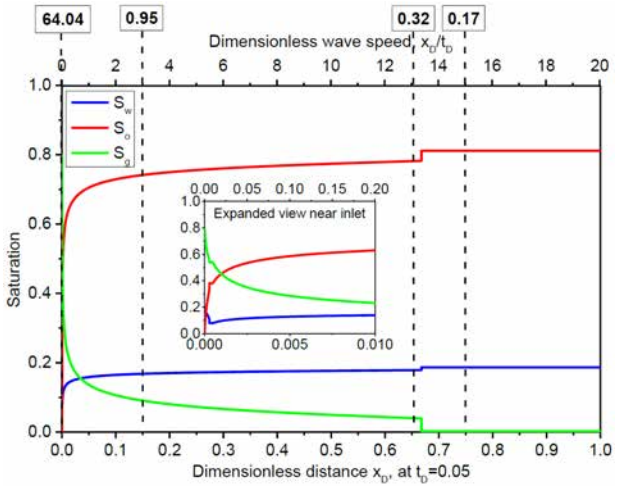

Figure 5—(Right). Saturation velocities (on the top axis) along the path in Fig. 4 and phase distribution (on the bottom axis) at time *tD* = 0.05 PVI. The boxed numbers labelled on the top are total relative mobilities λ_{rt} (Eq. 13) in units (1/cp) at that position.

Figure 5 displays the velocities of the saturations along the path in Fig. 4 and phase distribution at *tD* = 0.05 PVI, which is obtained by multiplying saturation velocities with *tD*. The numbers labelled on the top specify the total relative mobility λ_{rt} at that position:

$$\lambda_{rt} = k_{rw}/\mu_w + k_{ro}/\mu_o + k_{rg}^f/\mu_g. \tag{13}$$

The phase distribution suggests gas (green profile) pushes oil (red profile) forward but extremely slowly, e.g. *n(So=0.1')* = 0.001, meaning 1000 PVI required to displace oil to this saturation. This is due to the fact that without foam gas is much more mobile than liquids. In addition, λ_{rt}, much greater upstream than downstream, indicates fingering would be expected in 2D or 3D media, restricting both sweep and trapping of gas.

Scenario 2 with Combination of J_{nf} and I_{fm}

Figure 6 illustrates the composition path for Case 1 of Scenario 2 in Table 1 for a combination of J_{nf} outside and *Ifm* inside the foam region. With this scenario, one may hope to create foam some distance from the injection well. This might correspond to a surfactant-alternating-gas (SAG) injection process with a single large gas slug injected following a single large surfactant slug.

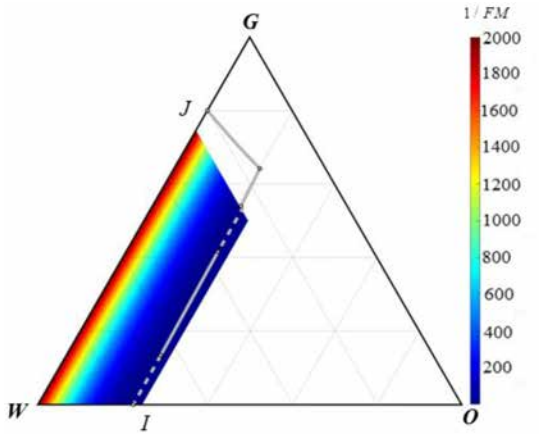

Figure 6—(Left). Composition path for Case 1 of Scenario 2 in Table 1 in ternary saturation space, with J_{nf} outside and *Ifm* just inside the foam region. Solid line marks a spreading wave and dashed line a shock.

The composition path starting from J_{nf} comprises two spreading waves outside the foam region and enters into the foam region with a shock. It is followed by a third spreading wave connected by a second shock to I_{fm} along the foam boundary at $S_o = fmoil$. This suggests foam is created away from the injection well, but substantially weakened by oil.

Figure 7 displays the velocities of saturations along the path in Fig. 6 and phase distribution at time t_D = 0.2 PVI. Oil is driven by gas but very inefficiently: more than 500 PVI required to reduce S_o to 0.1 ($\eta(S_o=0.1)$ = 0.002). However, λrt = 29.28 (1/cp) with foam near the well, which is 2.19 times less than 64.04 (1/cp) at J_{nf}. This suggests fingering of injected gas into the foam. Gas propagation is slowed down by 3.24 times, e.g. n = 4.12 in Fig. 7 and 13.35 in Fig. 5. The sweep of gas is improved, as seen from $S_g \sim 0.1$ at t_D = 1 in Scenario 1 but $S_g \sim 0.3$ in Scenario 2. Scenario 2, with its increased gas saturation, benefits CO_2 sequestration in oil reservoirs.

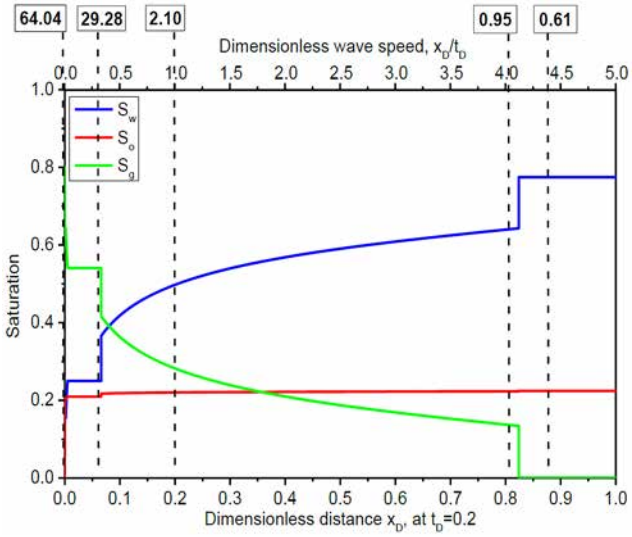

Figure 7—(Right). Saturation velocities (on the top axis) along the path in Fig. 6 and phase distribution (on the bottom axis) at t_D = 0.2 PVI. The boxed numbers are λrt (Eq. 13) in units (1/cp) at that position.

Scenario 3 with Combination of J_{fm} and I_{fm}. Figure 8 presents the composition path for Case 1 of Scenario 3 in Table 1 for a combination of J_{fm} and I_{fm} both inside the foam region. Most field applications correspond to this scenario, e.g. co-injection of foaming solution and gas or SAG injection to develop foam from or near the well.

The Scenario 3 follows, starting from J_{fm}, a spreading wave, an abrupt shock, a second short-spreading wave and eventually a second shock to I_{fm}. In contrast with J_{nf}, the whole path resides within the foam region, indicating foam is developed in the entire displacement.

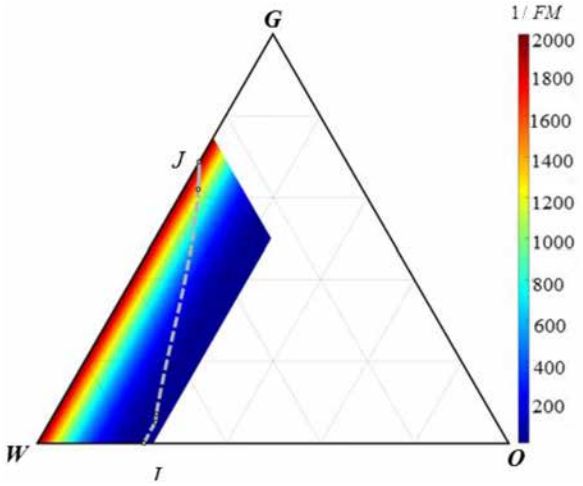

Figure 8—(Left). Composition path for Case 1 of Scenario 3 in Table 1 in ternary saturation space, with J_{fm} and I_{fm} both inside the foam region. A solid line denotes a spreading wave and a dashed line a shock.

Figure 9 shows the corresponding saturation velocities and phase distribution at $t_D = 0.2$. In the Scenario 3, oil is displaced by foam near the entrance, much more efficiently than in Scenarios 1 or 2. η (S_o=0.03) = 0.08, equivalent to 12.5 PVI to recover nearly all oil. For oil recovery in the field, such large injection volumes are still not practical. Nevertheless, the mobility control is very successful ($\lambda \boldsymbol{rt} < 1$ everywhere), benefiting CO_2 sequestration. Especially, foam in this scenario can improve sweep efficiency and increase gas saturation in the swept zone in 2D or 3D media, as seen from $S_g \sim 0.6$ at about 12.5 PVI.

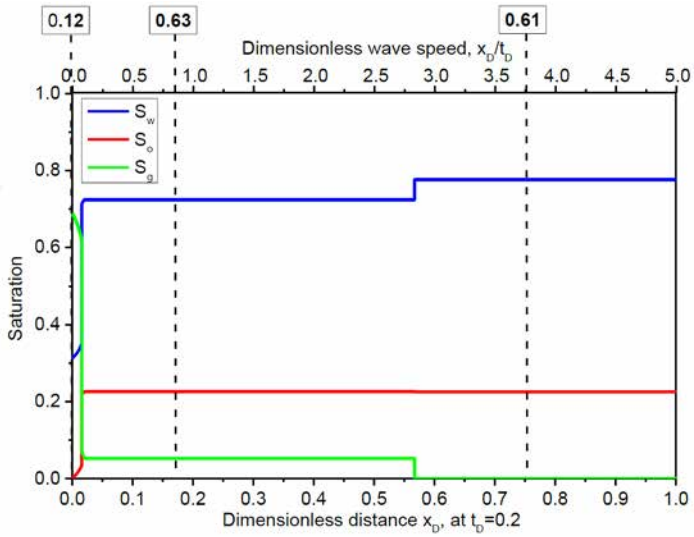

Figure 9—(Right). Saturation velocities (on the top axis) along the path in Fig. 8 and phase distribution (on the bottom axis) at t_D> = 0.2 PVI. The boxed numbers are λrt (Eq. 13) in units (1/cp) at that position.

Scenario 4 with Combination of J_{fm} and I_{nf}

Figure 10 shows the composition path for Case 1 of Scenario 4 in Table 1, for a combination of J_{fm} inside and I_{nf} outside the foam region. The path starting from J_{fm} crosses the foam boundary at $S_o = fmoil$, representing foam injection into a formation with initial S_o unstable for foam.

Figure 11 shows the saturation velocities along the path of Fig. 10 and phase distribution at tD = 0.1 PVI. The oil-displacement mechanism at the leading edge of the displacement is waterflooding, which displaces oil until So < fmoil, allowing the propagation of a stable foam bank. The foam bank propagates at velocity η = 0.08 (similar to Scenario 3), displacing water and oil ahead with a favourable mobility ratio of (0.12/0.63).

Nevertheless, the waterflooding may be subject to fingering, retaining a higher So in 2D or 3D media, and inhibiting the foam bank.

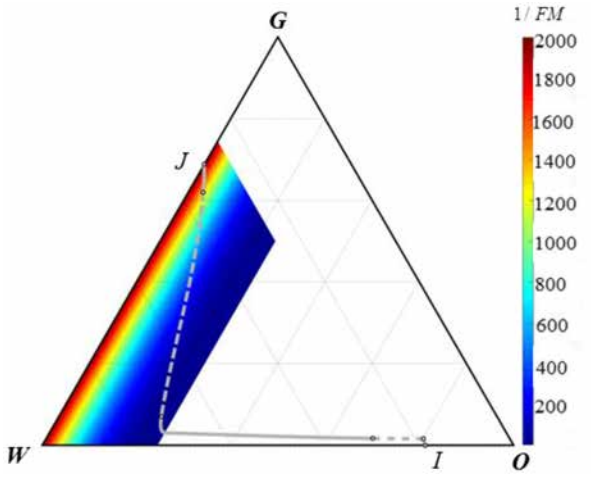

Figure 10—(Left). Composition path for Case 1 of Scenario 4 in Table 1 in ternary saturation space, with J_{fm} inside but I_{nf} outside the foam region. A solid line denotes a spreading wave and a dashed line a shock.

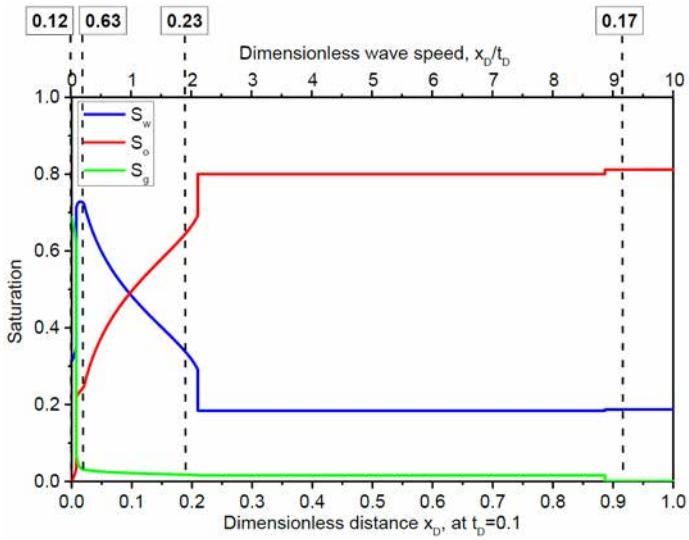

Figure 11—(Right). Saturation velocities (on the top axis) along the path in Fig. 10 and phase distribution (on the bottom axis) at t_D = 0.1 PVI. The boxed numbers are λ_{rt} (Eq. 13) in units (1/cp) at that position.

Effect of Improved Foam Tolerance to Oil

The results above suggest Scenarios 3 and 4 are more favorable for field applications. We present here an analysis of foam-oil flow behavior in the two scenarios, with a surfactant formulation more tolerant to oil.

Effect on Composition Path. The tolerance of foam to oil is characterized by oil-parameter *fmoil* as in Eq. A-8; a greater value of *fmoil* represents a foam more tolerant to oil. The effects of increasing foam tolerance to oil on the composition path and phase distribution with foam injection in Scenarios 3 and 4 are illustrated in Figs. 12 and 13 and Figs. 14 and 15, respectively. Increasing *fmoil* expands the foam region in both scenarios, suggesting that stable foam is allowed for a larger range of S_o.

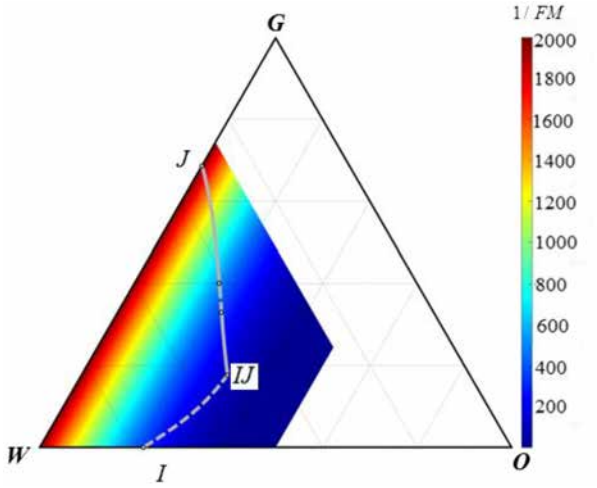

Figure 12—(Left). Composition path for Case 2 of Scenario 3 in Table 1 in ternary saturation space, with J_{fm} and I_{fm}. Parameter *fmoil* is increased to 0.5 relative to Case 1 in Fig. 8. A solid line denotes a spreading wave, and a dashed line a shock.

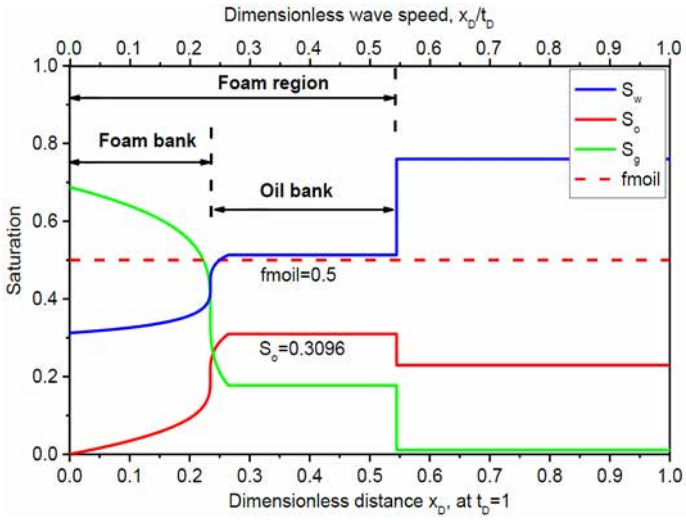

Figure 13—(Right). Saturation velocities (on the top axis) along the path of Fig. 12 and phase distribution (on the bottom axis) at t_D = 1 PVI. Note that S_o < *fmoil* within the oil bank ahead of the foam bank.

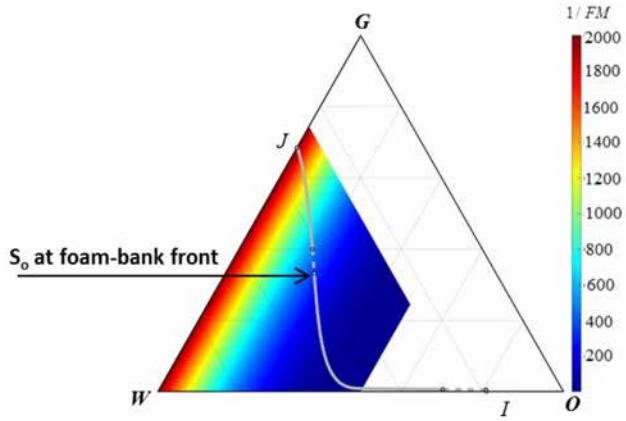

Figure 14—(Left). Composition path for Case 2 of Scenario 4 in Table 1 in ternary saturation space, with J_{fm} inside and I_{nf} outside the foam region. Parameter *fmoil* is increased to 0.5 relative to Case 1 in Fig. 10. A solid line denotes a spreading wave and a dashed line a shock.

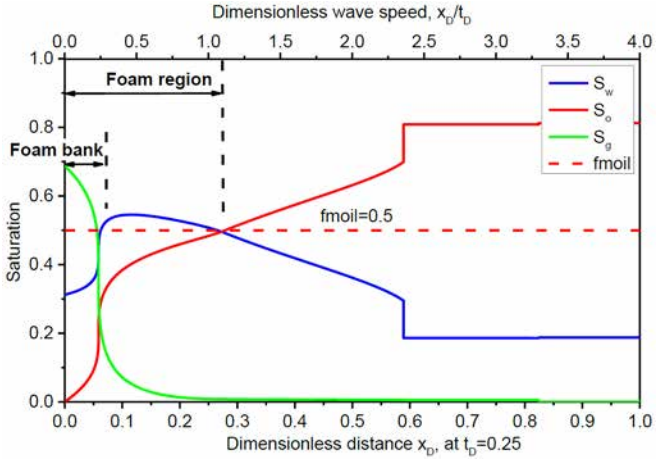

Figure 15—(Right). Saturation velocities (on the top axis) along the path of Fig. 14 and phase distribution (on the bottom axis) at t_D = 0.25 PVI. Note that S_o < *fmoil* immediately ahead of the foam bank.

In Scenario 3, with foam more stable to oil, an oil bank is created ahead of the foam bank, as seen in Fig. 13. The uniform state within the oil bank corresponds to the intermediate state *IJ* in Fig. 12, which is the intersection of the forward slow path from *J* and backward fast path from *I* (Liu, 1974; Castaneda et al., 2016). We note that the *IJ* state in Scenario 3 resides in the foam region. In other words, S_o in the oil bank nowhere exceeds the upper limit *fmoil* for stable foam. The generality of this finding ($S_o < fmoil$ in the oil bank) is demonstrated by the following argument. Suppose that in Scenario 3, with a combination of J_{fm} and *Ifm*, foam creates an oil bank with S_o exceeding *fmoil*. Immediately behind the oil bank, foam is present and reduces gas mobility substantially, leading to water fractional flow $f_w >> 0$. Within the oil bank, gas mobility is high and S_o is high, resulting in $f_w \sim 0$. Nevertheless, S_w increases from the foam bank to the oil bank. The decrease in f_w and increase in S_w across the foam front implies negative velocities, i.e. $(\Delta f_w / \Delta S_w) < 0$. This is physically impossible as it violates the velocity compatibility required for a forward displacement (Lake et al., 2014).

Similar behavior is also found in Scenario 4, i.e. that immediately in front of the foam bank, $S_o <$ fmoil (see Fig. 15); this value of S_o corresponds the endpoint of the first shock (as labelled in Fig. 14), which resides inside the foam region. This suggests that foam development is possible with an initial state I_{nf} that does not allow stable foam, though it relies on waterflooding ahead to reduce S_o below *fmoil* ahead of the foam.

Nevertheless, in both scenarios, improving the foam tolerance to oil does not change the nature of the composition path. For instance, with *fmoil* increasing, the path in Scenario 3 still resides within the foam region (see Figs. 8 and 12), and the path in Scenario 4 crosses the foam region in the same manner (see Figs. 10 and 14). Furthermore, the wave type and sequence from injection to initial state remains the same in each scenario, regardless of the change in *fmoil*. Of course, increasing foam tolerance to oil may transform a case with I_{nf} to a case with I_{fm}, with a large benefit to mobilities, velocities and sweep efficiency.

Effect on Foam- and Oil-bank Propagation. Figure 16 shows the propagation of foam and oil banks in Scenario 3, with respect to oil-related parameters, upper- (*fmoil*) and lower-limiting (*floil*) oil saturation in Eq. A-8. In this scenario foam displaces an initial saturation S_o that allows foam. Similarly, Fig. 17 shows the effect of the same parameters on foam- and oil-bank propagation in Scenario 4. In this case foam displaces an initial saturation S_o that does not allow foam.

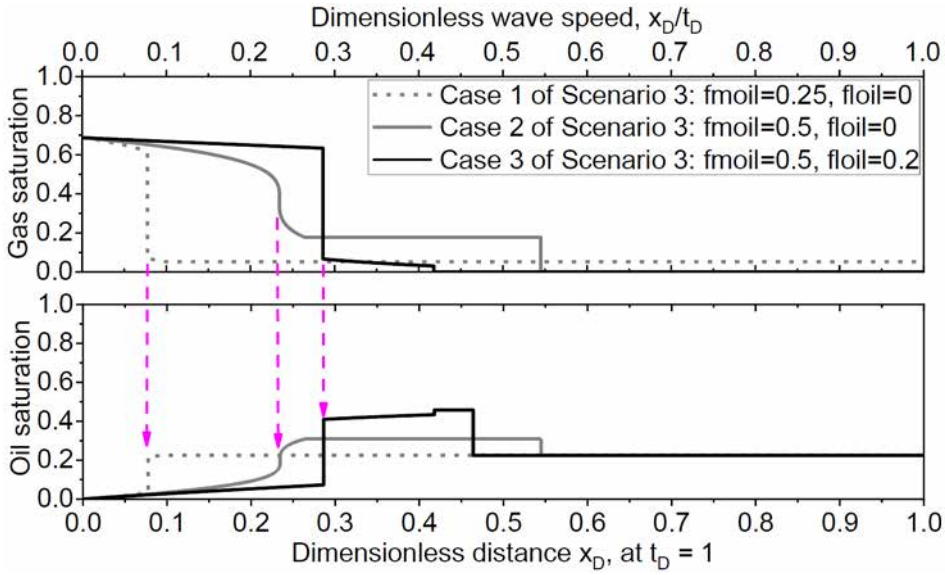

Figure 16—Saturation velocities (on the top axis) and phase distribution (on the bottom axis) at 1 PVI for gas (upper figure) and oil (lower figure) in Cases 1, 2 and 3 of Scenario 3 in Table 1, respectively. The arrows indicate the front of the foam and oil banks in each case.

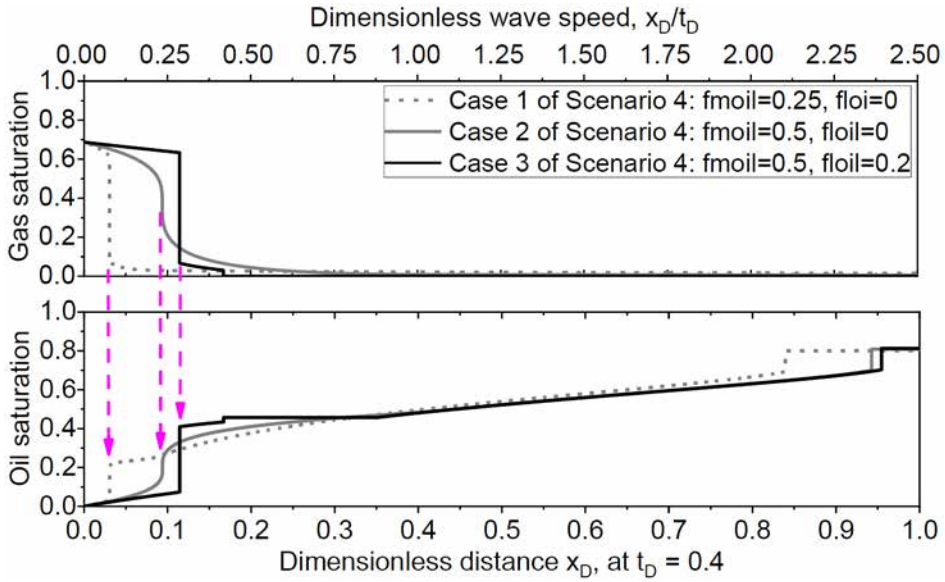

Figure 17—Saturation velocities (on the top axis) and phase distribution (on the bottom axis) at 0.4 PVI for gas (upper figure) and oil (lower figure) in Cases 1, 2 and 3 of Scenario 4 in Table 1, respectively. The arrows indicate the front of the foam bank in each case.

The S_g and S_o distributions suggest that increasing *fmoil* or *floil* (i.e., designing a surfactant formulation less sensitive to oil) accelerates the propagation of both foam and oil banks in either scenario. Greater foam tolerance to oil raises S_g in the foam bank and S_o in the oil bank. On the whole, it accelerates the production of most of the oil and increases S_g in the swept region.

Figures 16 and 17 also show that the foam bank propagates with nearly same velocity, 0.078 (dark- black line), 0.234 (light-grey line) or 0.287 (dashed line), for the same oil tolerance but different initial conditions, respectively. This suggests the propagation velocity of the foam bank may be not sensitive to an initial condition that allows foam or kills foam, but rather mainly to foam properties at the injection conditions.

Numerical artifact in Foam Simulation with Oil

We compare the analytical solutions and a numerical solution for foam flow with oil and find a possible numerical artifact in standard finite-difference simulation. Here we discuss the possible reason for the artifact.

Figure 18 shows the numerical simulation result for a 1D immiscible foam flow with oil from Liu et al. (2011) using the same STARS model approximations. *J* and *I* in the simulation of Liu et al. are both in the foam region, as in Scenario 3. In contradiction with the analytical solutions in Figs. 12 and 13, Fig. 18 shows that S_o within the oil bank chased by the foam bank exceeds *fmoil*, but the numerical solution still shows a propagation of foam.

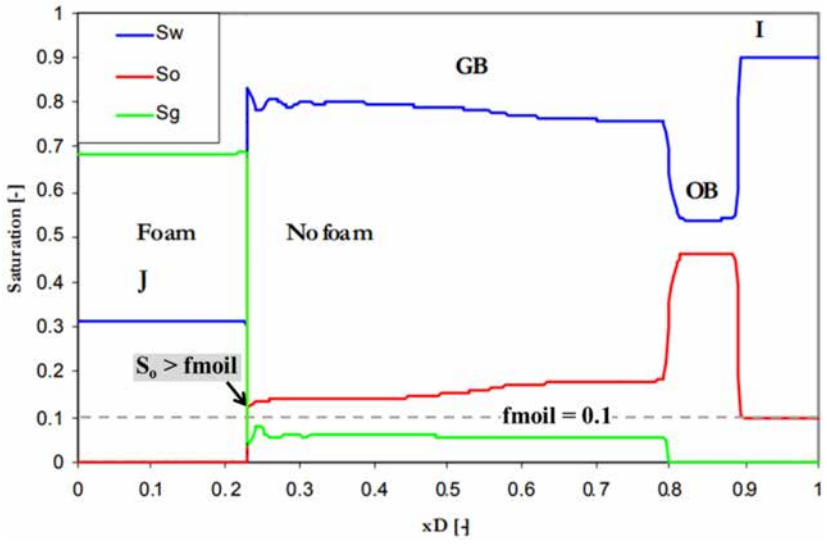

Figure 18—Numerical results for 1D immiscible foam flow with oil, adapted from Liu et al. (2011). Parameter *fmoil* used is 0.1 (implied by the dashed line). S_o within the oil bank is much greater than *fmoil*.

The propagation of foam with $S_o > fmoil$ ahead may arise from the calculation of pressure *p* or pressure gradient # *p* using neighboring grid blocks. As illustrated in Fig. 19, the interface between grid blocks *i* and (*i* - 1) corresponds to the foam-displacement front in Fig. 16. In numerical simulation, the *p* in grid block *i* is calculated using *p* in the neighboring grid (*i* - 1) with foam and grid (*i* + 1) without foam. *p* in the grid (*i* - 1) with foam should be much greater than that in the grid *i* without foam. This leads to an otherwise small *p* in grid *i* (without foam) greatly overestimated. The # *p* that regulates the flow of oil out of grid *i* is therefore greatly overestimated relative to its actual value with no foam. When S_o in the grid *i* is reduced (by the artificially inflated # *p*) to a value less than *fmoil*, foam advances to grid block *i*, misleadingly implying that foam can efficiently displace oil ahead of it with $S_o > fmoil$.

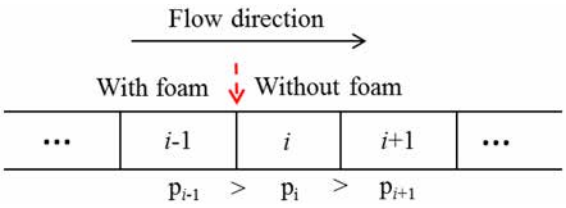

Figure 19—Schematic of pressure calculation using neighboring grid blocks in finite-difference simulation. The interface between grids (*i* -1) and *i* corresponds to the foam front in Fig. 16.

Conclusions

We present analytical solutions of composition paths for foam flow with oil for four representative scenarios with different combinations of injection (*J*) and initial (*I*) condition that sustains or kills foam. These analytical solutions can be used to guide the interpretation of foam-flow behavior with oil and as benchmarks for calibrating numerical simulators for foam simulations.

Scenarios 1 and 2, with injection state *J* that does not sustain foam, are undesirable in field applications of foam to oil recovery or CO2 sequestration, because of unsuccessful gas-mobility control. In 2D or 3D media, gas would finger through the medium, leaving a large portion of the medium unswept.

Scenarios 3 and 4, with *J* sustaining foam (e.g. co-injection or surfactant-alternating-gas injection), are most desirable in field applications. For Scenario 3 with *J* and *I* both sustaining foam, foam is developed in the entire displacement. For Scenario 4 with *J* sustaining foam but *I* unstable for foam, foam can also be developed but it has to rely on waterflooding ahead to reduce oil saturation till stable for foam.

Changing foam tolerance to oil does not change the wave structure of a composition path within Scenarios 3 and 4. However, improving the oil tolerance of foam benefits oil-bank creation, propagation velocity of foam and oil banks, and sweep efficiency in oil displacement and CO_2 storage in 3D reservoirs. The velocity of foam-bank propagation is controlled by foam properties at *J*, but independent of initial state. Much bigger benefits come if the increase in oil tolerance shifts the process from Scenario 4 to Scenario 3.

Analytical solutions show that oil saturation (S_o) within an oil bank (if created and displaced by foam) never exceeds the upper limit for stable foam, *fmoil*, which is justified by saturation-velocity considerations. The numerical solution for one case contradicts the analytical solution, showing $S_o > fmoil$ in the oil bank, reflecting a possible artifact in finite-difference simulation of foam with oil. This artifact possibly arises from the calculation of pressure or pressure gradient using neighboring grid blocks.

Acknowledgement

This project was funded (in part) by the United Arab Emirates University (Grant code: 12N099) and the National Council of Science and Technology (CONACYT) (Grant code: A1-S-26012). P. C. also thanks the Asociacion Mexicana de Cultura A.C. for the financial support.

References

Alvarez, J. M., Rivas, H. J., & Rossen, W. R. (2001). Unified model for steady-state foam behavior at high and low foam qualities. *SPE Journal*, **6**(03), 325–333.

Azevedo, A. V., de Souza, A. J., Furtado, F., Marchesin, D., & Plohr, B. (2010). The solution by the wave curve method of three-phase flow in virgin reservoirs. *Transport in Porous Media*, **53**(1), 99–125.

Ashoori, E., Marchesin, D., & Rossen, W. R. (2011). Roles of transient and local equilibrium foam behavior in porous media: Traveling wave. *Colloids and Surfaces A: Physicochemical and Engineering Aspects*, **377**(1-3), 228–242.

Ashoori, E., van der Heijden, T. L. M., & Rossen, W. R. (2010). Fractional-flow theory of foam displacements with oil. *SPE Journal*, **15**(02), 260–273.

Boeije, C. S., & Rossen, W. (2015). Fitting foam-simulation-model parameters to data: I. coinjection of gas and liquid. *SPE Reservoir Evaluation & Engineering*, **18**(02), 264–272.

Bertin, H., Estrada, E. D. C., & Atteia, O. (2017). Foam placement for soil remediation. *Environmental Chemistry*, **14**(5), 338–343.

Bui, M., Adjiman, C. S., Bardow, A., Anthony, E. J., Boston, A., Brown, S., … Hackett, L. A. (2018). Carbon capture and storage (CCS): the way forward. *Energy & Environmental Science*, **11**(5), 10621176.

Charbeneau, R. J. (1988). Multicomponent exchange and subsurface solute transport: Characteristics, coherence, and the Riemann problem. *Water Resources Research*, **24**(1), 57–64.

Cheng, L., Reme, A. B., Shan, D., Coombe, D. A., & Rossen, W. R. (2000). Simulating foam processes at high and low foam qualities. Presented at the SPE/DOE Improved Oil Recovery Symposium, Tulsa, Oklahoma, April 3-5, 2000.

Computer Modeling Group (Calgary, Alberta, Canada), STARS User's Guide, Version 2015. See also GEM User's Guide.

Castaneda, P., Abreu, E., Furtado, F., & Marchesin, D. (2016). On a universal structure for immiscible three-phase flow in virgin reservoirs. *Computational Geosciences*, **20**(1), 171–185.

Castaneda-Herrera, C. A., Stevens, G. W., & Haese, R. R. (2018). Review of CO2 leakage mitigation and remediation technologies. *Geological Carbon Storage: Subsurface Seals and Caprock Integrity*, **235**, 327.

Estrada, E. D. C., Bertin, H., & Atteia, O. (2015). Experimental study of foam flow in sand columns: surfactant choice and resistance factor measurement. *Transport in Porous Media*, **105**(2), 335–354.

Furtado, F. (1991). Structural stability of nonlinear waves for conservation laws. *Ph.D. dissertation*, New York University.

Farajzadeh, R., Andrianov, A., Krastev, R., Hirasaki, G. J., & Rossen, W. R. (2012). Foam-oil interaction in porous media: Implications for foam assisted enhanced oil recovery. *Advances in Colloid and Interface Science*, **183-184**, 1–13.

Glass, R. J., & Yarrington, L. (2003). Mechanistic modeling of fingering, nonmonotonicity, fragmentation, and pulsation within gravity/buoyant destabilized two-phase/unsaturated flow. *Water Resources Research*, **39**(3).

Kim, J. S., Dong., Y., and Rossen, W. R. (2005). "Steady-state flow behavior of CO2 foam," *SPE Journal* **10**, 405–415.

Liu, T. P. (1974). The Riemann problem for general 2* 2 conservation laws. *Transactions of the American Mathematical Society*, **199**, 89–112.

LaForce, T., & Johns, R. T. (2005). Analytical solutions for surfactant-enhanced remediation of nonaqueous phase liquids. *Water Resources Research*, **41**(10).

Liu, M., Andrianov, A., & Rossen, W. R. (2011). Sweep efficiency in CO2 foam simulations with oil. Presented at the IOR 2011 - 16th European Symposium on Improved Oil Recovery, Cambridge, UK, April 12-14, 2011.

Lake, L. W., Johns, R. T., Rossen, W. R., & Pope, G. (2014). Fundamentals of enhanced oil Recovery. Richard, Texas: Society of Petroleum Engineers.

Lyu, X., Voskov, D., Tang, J., & Rossen, W. R. (2021). Simulation of foam enhanced-oil-recovery processes using operator-based linearization approach. *SPE Journal*, **26**(04), 2287–2304.

Osterloh, W. T., & Jante, M. J., Jr. (1992). Effects of gas and liquid velocity on steady-state foam flow at high temperature. Presented at the SPE/DOE Enhanced Oil Recovery Symposium, Tulsa, Oklahoma, April 22-24, 1992.

Rossen, W. R. (1996). Foams in enhanced oil recovery. In foams: theory, measurements, and applications (pp. 413–464). MaRcel Dekker.

Rossen, W. R., Venkatraman, A., Johns, R. T., Kibodeaux, K. R., Lai, H., & Tehrani, N. M. (2011). Fractional flow theory applicable to non-Newtonian behavior in EOR processes. *Transport in Porous Media*, **89**(2), 213–236.

Rossen, W. R. (2013). Numerical challenges in foam simulation: a review. Presented at the SPE Annual Technical Conference and Exhibition, New Orleans, Louisiana, USA, September 30 - October 2, 2013.

Rossen, W. R., Farajzadeh, R., Hirasaki, G. J., & Amirmoshiri, M. (2022). Potential and challenges of foam-assisted CO2 sequestration. Presented at the SPE Improved Oil Recovery Conference, Tulsa, Oklahoma, April 25-29, 2022.

Reynolds, C., & Krevor, S. (2015). Characterizing flow behavior for gas injection: relative permeability of CO2-brine and N2-water in heterogeneous rocks. *Water Resources Research*, **51**(12), 9464–9489.

Schramm, L. L. (1994). Foams: fundamentals and applications in the petroleum industry. In Comstock M. Joan (Ed.) (Vol. **242**, pp. i–vii). American Chemical Society.

Tang, J., Vincent-Bonnieu, S., & Rossen, W. R. (2019a). Experimental investigation of the effect of oil on steady-state foam flow in porous media. *SPE Journal*, **24**(01), 140–157.

Tang, J., Ansari, M. N., & Rossen, W. R. (2019b). Quantitative modeling of the effect of oil on foam for enhanced oil recovery. *SPE Journal*, **24**(03) 1057–1075.

Tang, J., Castaneda, P., Marchesin, D., & Rossen, W. R. (2019c). Three-phase fractional-flow theory of foam-oil displacement in porous media with multiple steady states. *Water Resources Research*, **55**(12), 10319–10339.

You, K., DiCarlo, D., & Flemings, P. B. (2015). Quantifying hydrate solidification front advancing using method of characteristics. *Journal of Geophysical Research: Solid Earth*, **120**(10), 6681–6697.

Zhou, Z., & Rossen, W. R. (1995). Applying fractional-flow theory to foam processes at the "limiting capillary pressure." *SPE Advanced Technology Series*, **3**(1), 154–162.

Appendix A

Implicit-texture Foam Model

In the STARS model, foam modifies gas relative permeability, k_{rg} in Eq. 5, through a mobility-reduction factor *FM:*

where superscript *f* denotes the presence of foam.

$$k_{rg}^{f} = k_{rg} \cdot FM \tag{A-1}$$

FM comprises a series of functions F_i (i =1, 2, 3…), accounting for the impacts of a variety of factors on foam, e.g. surfactant concentration, water saturation, oil saturation, oil composition, shear-thinning behavior and salinity:

$$FM = \frac{1}{1 + fmmob \cdot F_1 \cdot F_2 \cdot F_3 \cdot F_4 \cdot F_5 \cdot F_6} \tag{A-2}$$

where *fmmob* is the reference gas-mobility-reduction factor, denoting the maximum attainable reduction in gas mobility. In this study, we consider two key functions, F_2, a function of S_w, and F_3, a function of S_o, to represent the effects of water and oil saturations. The factor *FM* is thus a function only of (Sw, S_o). The water-saturation-dependent function, F_2 in the wet-foam representation is defined as follows:

The water-saturation-dependent function, *F2* in the wet-foam representation is defined as follows:

$$F_2 = 0.5 + \frac{\arctan[epdry(S_w - fmdry)]}{\pi} \tag{A-3}$$

where *fmdry* denotes the limiting water saturation below which foam collapses; the abruptness of foam collapse is controlled by an adjustable parameter, *epdry*. Since experimental data demonstrate a sharp transition between the two flow regimes as in Figs. 1 and 2, a large value of *epdry* is assumed, giving an abrupt foam collapse at S_w around *fmdry*.

To simplify the calculation of derivatives of fractional flows in Eq. 11, F_2 in Eq. A-3 is approximated and replaced here by a fifth-order polynomial function $p(x)$:

$$p(x) = a + bx + cx^2 + dx^3 + ex^4 + fx^5 \tag{A-4}$$

where *a, b, c, d, e* and *f* are coefficients. Variable x is a function of Sw:

$$x = 2 \times epdry(S_w - fmdry) \tag{A-5}$$

where parameters *epdry* and *fmdry* here have the same definitions as in Eq. A-3.

The following six conditions are used to solve for the six coefficients in Eq. A-4:

$$\begin{cases} p(-1) = 0; & p(-1) = 1; \\ p(-1) = 0; & p(1) = 0; \\ p'(-1) = 0; & p'(-1) = 0; \end{cases} \tag{A-6}$$

Equation A-3, for the impact of S_w on foam, is then replaced by the following polynomial function:

$$\begin{cases} p(x) = 0 & x < -1 \\ p(x) = \frac{1+1.875x-1.25x^3+0.375x^5}{2} & -1 \le x \le 1 \\ p(x) = 1 & x > 1 \end{cases} \tag{A-7}$$

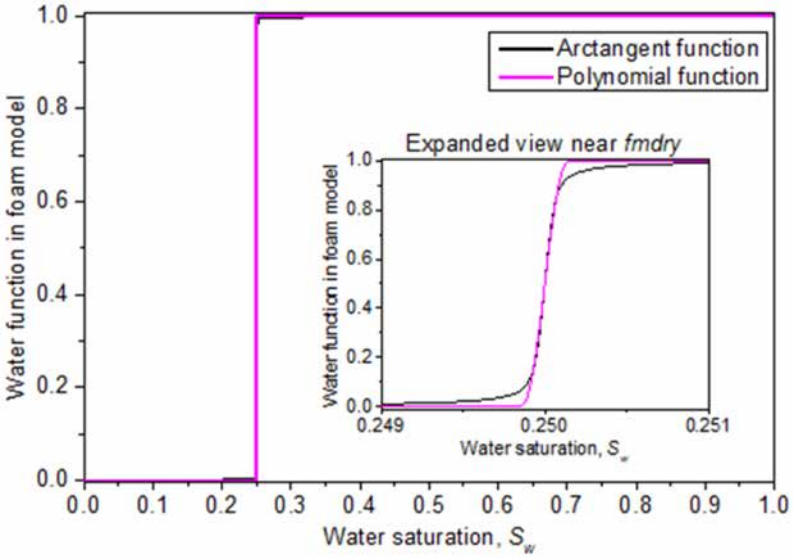

Figure A-1—Comparison between the arctangent function F_2 in Eq. A-3 and polynomial approximation $p(x)$ in Eq. A-7. Parameters are referred to Table A-1.

Figure A-1 plots F_2 in Eq. A-3 and its polynomial approximation $p(x)$ in Eq. A-7, using the parameters in Table A-1. The difference between the two functions is negligibly small, confirming that Eq. A-7 approximates accurately Eq. A-3 for the impact of S_w on foam. One difference is that foam collapses completely in this approximation at $S_w = \{fmdry - [1/(2\times epdry)]\}$, whereas foam does not collapse completely at any value of S_w in Eq. A-3.

The oil-saturation-dependent function F_3 is given by

$$F_3 = \begin{cases} 1 & S_{or} \le S_o \le floil \\ \left(\frac{fmoil - S_o}{fmoil - floil}\right)^{epoil} & floil < S_o < fmoil \\ 0 & fmoil \le S_o \le S_{wc} - S_{gr} \end{cases} \quad \text{(A-8)}$$

where *epoil* is the oil exponent and *fmoil* and *floil* are the upper- and lower-limiting oil saturations, respectively. For $S_{or} < S_o < floil$, $F_3 = 1$, suggesting oil has no impact on foam; for $S_o > fmoil$, $F_3 = 0$, indicating oil destroys foam completely; for $floil < S_o < fmoil$, F_3 decreases non-linearly from 1 to 0 with increasing S_o, representing a non-linear destabilizing effect of oil on foam.

Table A-1 gives the values of parameters in Corey-type relative-permeability model and foam model. The same parameter values are utilized, except for those specified in Table 1. We use a value for *fmmob* less than that obtained in the laboratory (Boeije and Rossen, 2015; Cheng et al., 2000), to account for weaker foam due to field complexities, e.g. adverse wettability, high salinity or high temperature.

Table A-1—A summary of parameter values used in the Corey relative-permeability and foam models.

Corey parameters and fluid properties						Foam model parameters		
k^o_{rw}	k^o_{ro}	k^o_{rg}	nw	no	ng	fmmob	fmdry	epdry
1	1	1	2	2	2	2000	0.3	3200
S_{wc}	S_{or}	s_{gr}	μ_w, cp	μ_o, cp	μ_g, cp	*fmoil*	*floil*	*epoil*
0.1	0.1	0	1	5	0.01	0.3	0.1	3

Note saturations and saturation-related factors shown here are original values without being normalized, while in Figs. 3 - 17, they are all normalized using Eq. 9.